A&A 612, A13 (2018)
DOI: 10.1051/0004-6361/201730581

Astronomy & Astrophysics
Special issue

H.E.S.S. phase-I observations of the plane of the Milky Way

HESS J1741−302: a hidden accelerator in the Galactic plane

H.E.S.S. Collaboration: H. Abdalla[1], A. Abramowski[2], F. Aharonian[3,4,5], F. Ait Benkhali[3], E. O. Angüner[21,⋆], M. Arakawa[41], C. Armand[24], M. Arrieta[15], M. Backes[8], A. Balzer[9], M. Barnard[1], Y. Becherini[10], J. Becker Tjus[11], D. Berge[36], S. Bernhard[13], K. Bernlöhr[3], R. Blackwell[14], M. Böttcher[1], C. Boisson[15], J. Bolmont[16], S. Bonnefoy[36], P. Bordas[3], J. Bregeon[17], F. Brun[26], P. Brun[18], M. Bryan[9], M. Büchele[35], T. Bulik[19], M. Capasso[28], S. Caroff[29], A. Carosi[24], S. Casanova[21,3,⋆], M. Cerruti[16], N. Chakraborty[3], R. C. G. Chaves[17,22], A. Chen[23], J. Chevalier[24], S. Colafrancesco[23], B. Condon[26], J. Conrad[27,⋆⋆], I. D. Davids[8], J. Decock[18], C. Deil[3], J. Devin[17], P. deWilt[14], L. Dirson[2], A. Djannati-Ataï[30], A. Donath[3], L.O'C. Drury[4], J. Dyks[33], T. Edwards[3], K. Egberts[34], G. Emery[16], J.-P. Ernenwein[20], S. Eschbach[35], C. Farnier[27,10], S. Fegan[29], M. V. Fernandes[2], A. Fiasson[24], G. Fontaine[29], S. Funk[35], M. Füßling[36], S. Gabici[30], Y. A. Gallant[17], T. Garrigoux[1], F. Gaté[24], G. Giavitto[36], D. Glawion[25], J. F. Glicenstein[18], D. Gottschall[28], M.-H. Grondin[26], J. Hahn[3], M. Haupt[36], J. Hawkes[14], G. Heinzelmann[2], G. Henri[31], G. Hermann[3], J. A. Hinton[3], W. Hofmann[3], C. Hoischen[34], T. L. Holch[7], M. Holler[13], D. Horns[2], A. Ivascenko[1], H. Iwasaki[41], A. Jacholkowska[16], M. Jamrozy[37], D. Jankowsky[35], F. Jankowsky[25], M. Jingo[23], L. Jouvin[30], I. Jung-Richardt[35], M. A. Kastendieck[2], K. Katarzyński[38], M. Katsuragawa[42], U. Katz[35], D. Kerszberg[16], D. Khangulyan[41], B. Khélifi[30], J. King[3], S. Klepser[36], D. Klochkov[28], W. Kluźniak[33], Nu. Komin[23], K. Kosack[18], S. Krakau[11], M. Kraus[35], P. P. Krüger[1], H. Laffon[26], G. Lamanna[24], J. Lau[14], J. Lefaucheur[15], A. Lemière[30], M. Lemoine-Goumard[26], J.-P. Lenain[16], E. Leser[34], T. Lohse[7], M. Lorentz[18], R. Liu[3], R. López-Coto[3], I. Lypova[36], D. Malyshev[28], V. Marandon[3], A. Marcowith[17], C. Mariaud[29], R. Marx[3], G. Maurin[24], N. Maxted[14,43], M. Mayer[7], P. J. Meintjes[39], M. Meyer[27,45], A. M. W. Mitchell[3], R. Moderski[33], M. Mohamed[25], L. Mohrmann[35], K. Morå[27], E. Moulin[18], T. Murach[36], S. Nakashima[42], M. de Naurois[29], H. Ndiyavala[1], F. Niederwanger[13], J. Niemiec[21], L. Oakes[7], P. O'Brien[32], H. Odaka[42], S. Ohm[36], M. Ostrowski[37], I. Oya[36], M. Padovani[17], M. Panter[3], R. D. Parsons[3], N. W. Pekeur[1], G. Pelletier[31], C. Perennes[16], P.-O. Petrucci[31], B. Peyaud[18], Q. Piel[24], S. Pita[30], V. Poireau[24], D. A. Prokhorov[23], H. Prokoph[12], G. Pühlhofer[28], M. Punch[30,10], A. Quirrenbach[25], S. Raab[35], R. Rauth[13], A. Reimer[13], O. Reimer[13], M. Renaud[17], R. de los Reyes[3], F. Rieger[3,40], L. Rinchiuso[18], C. Romoli[4], G. Rowell[14], B. Rudak[33], C. B. Rulten[15], V. Sahakian[6,5], S. Saito[41], D. A. Sanchez[24], A. Santangelo[28], M. Sasaki[35], R. Schlickeiser[11], F. Schüssler[18], A. Schulz[36], U. Schwanke[7], S. Schwemmer[25], M. Seglar-Arroyo[18], A. S. Seyffert[1], N. Shafi[23], I. Shilon[35], K. Shiningayamwe[8], R. Simoni[9], H. Sol[15], F. Spanier[1], M. Spir-Jacob[30], Ł. Stawarz[37], R. Steenkamp[8], C. Stegmann[34,36], C. Steppa[34], I. Sushch[1], T. Takahashi[42], J.-P. Tavernet[16], T. Tavernier[18], A. M. Taylor[36], R. Terrier[30], L. Tibaldo[3], D. Tiziani[35], M. Tluczykont[2], C. Trichard[20], M. Tsirou[17], N. Tsuji[41], R. Tuffs[3], Y. Uchiyama[41], D. J. van der Walt[1,⋆], C. van Eldik[35], C. van Rensburg[1], B. van Soelen[39], G. Vasileiadis[17], J. Veh[35], C. Venter[1], A. Viana[3,44], P. Vincent[16], J. Vink[9], F. Voisin[14], H. J. Völk[3], T. Vuillaume[24], Z. Wadiasingh[1], S. J. Wagner[25], P. Wagner[7], R. M. Wagner[27], R. White[3], A. Wierzcholska[21], P. Willmann[35], A. Wörnlein[35], D. Wouters[18], R. Yang[3], D. Zaborov[29], M. Zacharias[1], R. Zanin[3], A. A. Zdziarski[33], A. Zech[15], F. Zefi[29], A. Ziegler[35], J. Zorn[3], N. Żywucka[37], NANTEN Collaboration, R. Enokiya[46], Y. Fukui[46], T. Hayakawa[46], T. Okuda[47], K. Torii[46], and H. Yamamoto[46]

(Affiliations can be found after the references)

Received 8 February 2017 / Accepted 24 October 2017

ABSTRACT

The H.E.S.S. Collaboration has discovered a new very high energy (VHE, $E > 0.1$ TeV) γ-ray source, HESS J1741−302, located in the Galactic plane. Despite several attempts to constrain its nature, no plausible counterpart has been found so far at X-ray and MeV/GeV γ-ray energies, and the source remains unidentified. An analysis of 145-h of observations of HESS J1741−302 at VHEs has revealed a steady and relatively weak TeV source (∼1% of the Crab Nebula flux), with a spectral index of $\Gamma = 2.3 \pm 0.2_{\rm stat} \pm 0.2_{\rm sys}$, extending to energies up to 10 TeV without any clear signature of a cut-off. In a hadronic scenario, such a spectrum implies an object with particle acceleration up to energies of several hundred TeV. Contrary to most H.E.S.S. unidentified sources, the angular size of HESS J1741−302 is compatible with the H.E.S.S. point spread function at VHEs, with an extension constrained to be below 0.068° at a 99% confidence level. The γ-ray emission detected by H.E.S.S. can be explained both within a hadronic scenario, due to collisions of protons with energies of hundreds of TeV with dense molecular clouds, and in a leptonic scenario, as a relic pulsar wind nebula, possibly powered by the middle-aged (20 kyr) pulsar PSR B1737−30. A binary scenario, related to the compact radio source 1LC 358.266+0.038 found to be spatially coincident with the best fit position of HESS J1741−302, is also envisaged.

Key words. gamma rays: ISM – gamma rays: general – cosmic rays – ISM: clouds

1. Introduction

The H.E.S.S. Galactic Plane Survey (HGPS) catalog (H.E.S.S. Collaboration 2018b) contains 78 sources of very high energy (VHE) γ-rays, of which nearly 90% have been associated with at least one plausible counterpart in multi-wavelength catalogs. Pulsar wind nebulae (PWNe) appear to be the most prevalent VHE source class in the Galaxy, but there are also a sizable number of associations with supernova remnants (SNRs) and a handful of γ-ray binary systems. Many of the VHE sources have multiple associations, however, and it remains a major challenge to disentangle these and pinpoint the physical origin of the observed emission. Currently less than half of the sources in the HGPS catalog can be considered firmly identified. HESS J1741−302 is one of the most challenging VHE sources in this regard.

A preliminary detection of HESS J1741−302 was previously announced by H.E.S.S. (Tibolla et al. 2008) with an integrated flux level of ∼1% of the Crab Nebula flux above 1 TeV,

⋆ Corresponding authors: H.E.S.S. Collaboration, e-mail: contact.hess@hess-experiment.eu
⋆⋆ Wallenberg Academy Fellow.

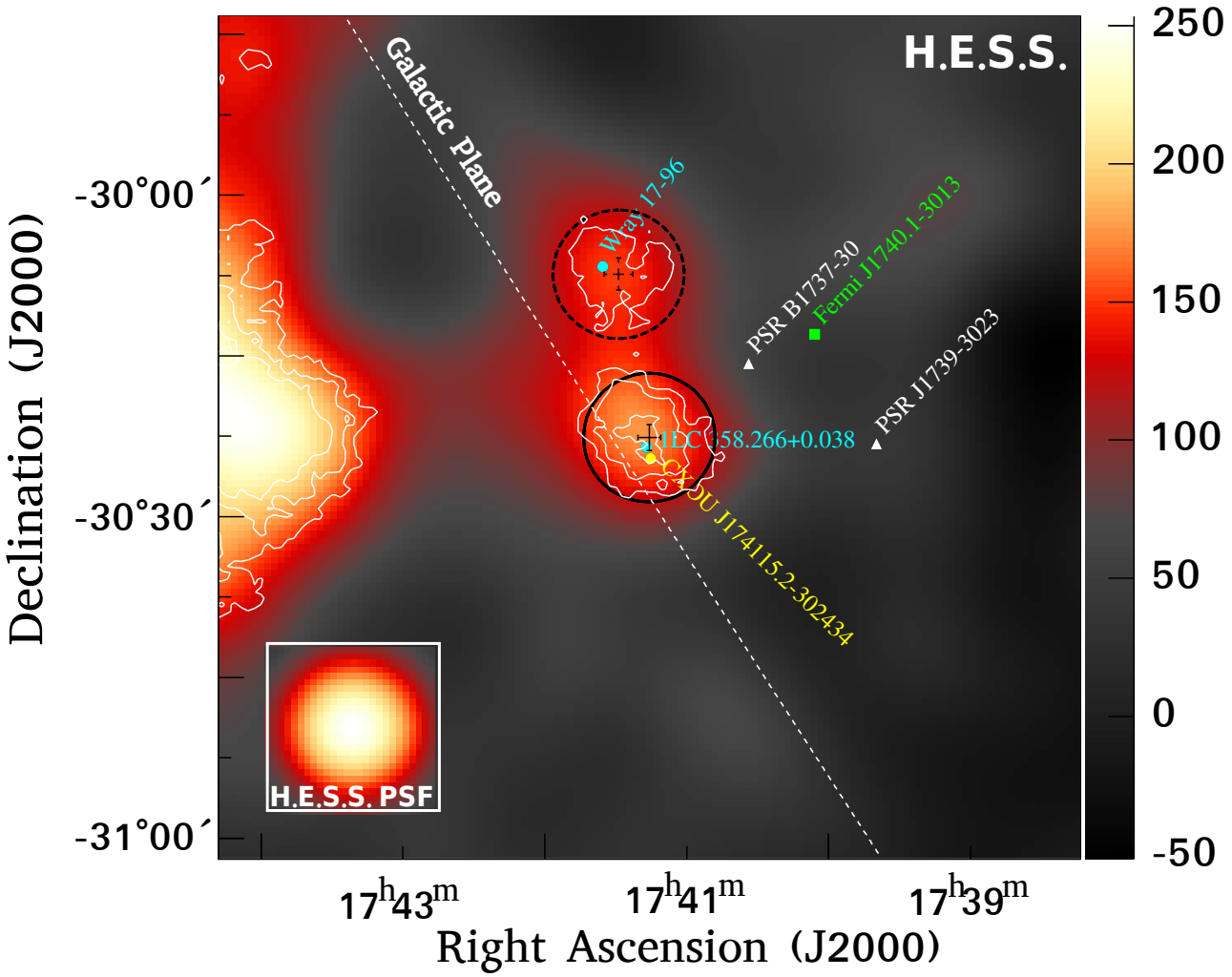

Fig. 1. γ-ray excess map of the region around HESS J1741−302, smoothed with a Gaussian kernel of 0.08° width chosen to match the H.E.S.S. PSF which is shown inside the white box in the bottom left corner. The color scale is in units of excess γ-rays per smoothing Gaussian width. The black circle shows the source region used for extracting the spectrum, while the black cross indicates the value and 1σ error interval (including systematic uncertainties) of the best fit position of the source. Similarly, the dashed black circle shows the hotspot region, while the dashed black cross indicates the value and 1σ error interval of the best fit position of this emission. The pulsars listed in Table 1 are marked with white triangles. The light blue dots mark the position of the compact radio source 1LC 358.266+0.038 and the LBV star Wray 17−96, while the green dot marks the best fit position of Fermi J1740.1−3013, respectively. The yellow circle show the location of the Chandra X-ray source *CXOU* J174115.2−302434. The white dashed line indicates the orientation of the Galactic plane, while the white contours show 5σ, 6σ and 7σ (pre-trial) statistical significance of the VHE γ-ray emission.

HESS J1741−302 is not only unidentified but also one of the ∼10% of VHE sources lacking even a promising association in the HGPS catalog. Thanks to the increased amount of high-quality VHE data and improved analysis techniques employed in this study, leading to a better sensitivity and angular resolution with respect to the previous analysis, the morphology and spectrum of HESS J1741−302 can now be characterized in detail for the first time, and opens up the possibility for deeper multi-wavelength follow-up observations of the source.

The region around HESS J1741−302 is rather complex as shown in Fig. 1, harboring two pulsars[1] as listed in Table 1, the OH/IR star OH 358.23+0.11 (Caswell 1998), a binary system, WR98a (Monnier et al. 1999), which is included in the Particle-Accelerating Colliding Wind Binaries catalog (De Becker & Raucq 2013), and a luminous blue variable (LBV) star[2], Wray 17−96 (Clark et al. 2005). In addition, a compact radio source, 1LC 358.266+0.038 (Nord et al. 2004) and a variable star, 2MASS J17411910−3023043[3] (Cutri et al. 2003), are found to be spatially coincident with the best fit position of HESS J1741−302. This non-thermal radio source, whose nature is still uncertain, is most likely a synchrotron emitter, displaying a spectral index of $\alpha = 1.1$ in its integrated flux density (when $S \propto \nu^{-\alpha}$). No variability is known for the compact radio object 1LC 358.266+0.038. On the other hand, the spectral energy distribution of the variable 2MASS star indicates that it might be a late type variable star.

[1] Note that there is another pulsar, PSR J1741−3016, located ∼0.1° away from the best fit position of HESS J1741−302. The VHE emission scenarios related to this pulsar are excluded since it is extremely old ($\tau_c = \sim 3.3$ Myr) and has a very low spin-down luminosity of 5.2×10^{31} erg/s.

[2] Note that there are less than 20 LBV stars known in the Galaxy with their remarkable mass-loss rates, while there are only a few TeV sources found in the vicinity of LBV stars (H.E.S.S. Collaboration 2018a).

[3] Note that the 2MASS star and the compact radio object are not positionally coincident.

Table 1. Pulsars around HESS J1741−302 with their properties.

Pulsar name	Position (J2000)	τ_c (kyr)	D_{PSR} (kpc)	Offset (°)	Separation (pc)	$\dot{E}$ (erg/s)	$\dot{E}/D^2_{PSR}$ (erg/s/kpc^2)	$L_\gamma/\dot{E}$ (%)
PSR B1737−30	RA: $17^h40^m33.8^s$	20.6	0.4	0.19	1.3	8.2×10^{34}	5.1×10^{35}	0.03
	Dec: −30°15′43.2″		3.28		10.9		7.6×10^{33}	1.84
PSR J1739−3023	RA: $17^h39^m39.8^s$	159	3.41	0.35	20.8	3.0×10^{35}	2.6×10^{34}	0.54
	Dec: −30°23′12.0″							

Notes. Pulsar data were taken from Manchester et al. (2005). The position column indicates the positions of pulsars, while the columns labeled τ_c and D_{PSR} show the characteristic age and the pulsar dispersion measure distance, respectively. The offset and separation columns show the relative offset of the pulsars with respect to the best fit position of HESS J1741−302 and the corresponding physical separation for the given pulsar distances, respectively. The $\dot{E}$ and $\dot{E}/D^2_{PSR}$ columns give the spin-down luminosity and flux of pulsars, respectively. The column labeled as $L_\gamma/\dot{E}$ gives the VHE γ-ray efficiencies of pulsars.

Dedicated observations of HESS J1741−302 at X-rays and high-energy (HE, 0.1−100 GeV) γ-rays did not result in any obvious counterpart. The source region has been observed by the *Suzaku* (Mitsuda et al. 2007), *Chandra* (Schwartz 2004) and *Swift* X-ray (Burrows et al. 2005) telescopes. The *Suzaku* observations (Uchiyama et al. 2011) showed no significant X-ray emission neither from the HESS J1741−302 region nor from the position of PSR B1737−30 after investigation of 46.2 ks of data. In that study, the X-ray flux upper limits for the HESS J1741−302 region and the pulsar were provided as $F_{\text{X-ray, HESS J1741−302}}$ (1−9 keV) $< 1.6 \times 10^{-13}$ erg s^{-1} cm^{-2} and $F_{\text{X-ray, PSR B1737−30}}$ (1−9 keV) $< 3.5 \times 10^{-13}$ erg s^{-1} cm^{-2} at a 90% confidence level, respectively. A recent investigation of the *Chandra* X-ray data[4] (Hare et al. 2016) did not yield any obvious counterpart for the TeV emission. The X-ray source *CXOU* J174115.2−302434, which is confidently classified as a star, is located within 2σ error interval of the best fit position of HESS J1741−302. In that study, scenarios related to active galactic nuclei were ruled out due to low X-ray to TeV flux ratio.

At HE γ-rays, there is no catalogued source coincident with the position of the H.E.S.S. source (Acero et al. 2015; Ackermann et al. 2016). A recent investigation of the *Fermi* LAT data has revealed a new HE source Fermi J1740.1−3013 (Hui et al. 2016) which is ∼0.3° offset from the best fit position of HESS J1741−302. In that study, the authors suggested a possible association between the HE source and both the pulsars PSR B1737−30 and PSR J1739−3023 since the curved spectrum of the new HE source resembles γ-ray pulsars, although the spectral parameters could not be tightly constrained.

In this paper, the analysis of a large 145-h VHE dataset on HESS J1741−302, obtained in part due to a relative proximity to the deep observed Galactic center, are presented with the aim to constrain the nature of this "hidden accelerator". Section 2 describes the details of VHE data analysis and presents the results. Section 3 describes a dedicated analysis of ^{12}CO and HI data from the interstellar medium (ISM) along the line of sight toward HESS J1741−302, which has been performed to investigate the possible hadronic origin of the observed emission. The results are discussed in Sect. 4, in which the potential origin of the faint VHE emission from HESS J1741−302 is considered in detail, with particular focus on the underlying particle acceleration mechanisms responsible for the production of γ-rays in both hadronic and leptonic scenarios.

[4] Two different dataset of 19.7 ks and 44.4 ks, coming from different observation regions, were investigated.

2. H.E.S.S. data analysis and results

2.1. The H.E.S.S. telescopes

The High Energy Stereoscopic System (H.E.S.S.) is an array of five imaging atmospheric Cherenkov telescopes located in the Khomas Highland of Namibia, 1800 m above sea level. H.E.S.S. in phase I comprised four 12 m diameter telescopes which have been fully operational since 2004. A fifth telescope (CT5), with a larger mirror diameter of 28 m and newly designed camera (Bolmont et al. 2014), was added in the center of the array and has been operational since September 2012. The H.E.S.S. phase I array configuration is sensitive to γ-ray energies between 100 GeV and several tens of TeV. The VHE H.E.S.S. data presented in this paper were taken with the H.E.S.S. phase I array configuration, which can measure extensive air showers with an angular resolution better than 0.1° and an average energy resolution of 15% for an energy of 1 TeV (Aharonian et al. 2006c).

2.2. Detection and morphological analysis

The observations of the field of view around HESS J1741−302 were carried out between 2004 and 2013, corresponding to an acceptance corrected live-time of 145 h of H.E.S.S. phase I data after the application of the quality selection criteria (Aharonian et al. 2006c). The data have been analyzed with the H.E.S.S. analysis package for shower reconstruction and the multivariate analysis technique (Ohm et al. 2009) has been applied for providing an improved discrimination between hadrons and γ-rays. Using this dataset, HESS J1741−302 is detected with a statistical significance of 7.8σ pre-trials (Li & Ma 1983), which corresponds to a 5.4σ post-trial. In order to provide improved angular resolution and reduce contamination from the bright and nearby source HESS J1745−303 (Aharonian et al. 2006b), the source position and morphology have been obtained with a hard cut configuration which requires a minimum of 160 photo-electrons per image. The cosmic-ray background level was estimated using the ring background model (Berge et al. 2007). Figure 1 shows the acceptance corrected and smoothed VHE γ-ray excess map of the region around HESS J1741−302, also indicating the locations of known astronomical objects.

For the morphology analysis, various models, including symmetric and asymmetric 2D Gaussian functions and a combination of these, convolved with the H.E.S.S. point spread function (PSF), were fitted to the excess map by using the Sherpa fitting package (Freeman et al. 2001). The H.E.S.S. PSF used in the morphology analysis was modeled as a weighted sum

Table 2. Results of the HESS J1741−302 morphology analysis.

Morphology model	RA (J2000)	Dec (J2000)	Extension (°)	LogLikelihood	χ^2/ndf (p-value)
Model A				23 677.2	14 783.3/14 653
HESS J1741−302	$17^h41^m15.4^s \pm 3.6^s_{stat}$	$-30°22'37.4'' \pm 51''_{stat}$	$0.032 \pm 0.018_{stat}$		(0.22)
Contamination	$17^h42^m49.8^s \pm 42.2^s_{stat}$	$-30°09'56.4'' \pm 4.4'_{stat}$	$0.409 \pm 0.089_{stat}$		
Model B				23 664.9	14 764.4/14 649
HESS J1741−302	$17^h41^m15.8^s \pm 3.6^s_{stat}$	$-30°22'37.2'' \pm 50''_{stat}$	$0.041 \pm 0.018_{stat}$		(0.25)
Contamination	$17^h43^m46.3^s \pm 79.2^s_{stat}$	$-30°07'43.1'' \pm 6.8'_{stat}$	$0.498 \pm 0.121_{stat}$		
Hotspot structure	$17^h41^m28.8^s \pm 4.5^s_{stat}$	$-30°07'22.5'' \pm 66''_{stat}$	$0.019 \pm 0.012_{stat}$		

Notes. The column labeled Morphology model shows the model components used for modeling the HESS J1741−302 region, while the columns labeled RA, Dec and Extension indicate the best fit position and the extension of the corresponding model component, respectively. The LogLikelihood column gives the log-likelihood value of the combined model used for comparing the tested models, while the χ^2/ndf column gives the chi-square test for goodness of fit along with the corresponding p-value. Note that each model component has four free parameters.

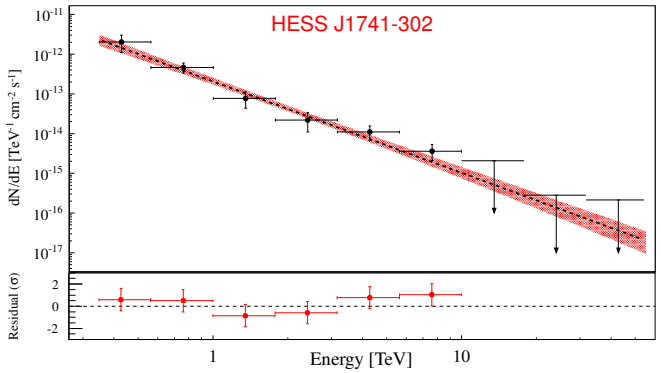

Fig. 2. VHE γ-ray spectrum of HESS J1741−302 extracted from the source region shown in Fig. 1. The black dots show the flux points with 1σ errors, while the red shaded region represents the 68% confidence interval for the fitted spectral model (between 0.4 TeV and 56.2 TeV). The dashed black line shows the best fit power-law function. The differential flux upper limits are at the 99% confidence level and are shown with arrows. The spectrum shown is binned in such a way that all points have a minimum significance level of 2.0σ. The significance of the last point is 2.8σ.

of three 2D Gaussian functions. The morphology models were compared using a log-likelihood ratio test (LLRT). The results of the morphology analysis are given in Table 2 along with the tested morphology models. The tested morphology models include three 2D Gaussians: one for describing the contamination coming from HESS J1745−303 (tagged as "Contamination" in Table 2), one for HESS J1741−302 and the other one for compensating the hotspot structure seen in the analysis residual map after fitting the previous two components (Model A). Although Model B improved the fit by 4.0σ (from LLRT) with respect to Model A, this improvement is not enough to claim the hotspot structure[5] as a new VHE γ-ray source, which would require a detection at a statistical significance above 5σ after trial corrections. This hotspot feature is interesting but after trials consistent with a statistical fluctuation, thus requiring deeper observations to confirm. The best fit centroid position of the 2D Gaussian representing HESS J1741−302 is RA (J2000): $17^h41^m15.4^s \pm 3.6^s_{stat} \pm 1.3^s_{sys}$ and Dec (J2000): $-30°22'37.4'' \pm 51''_{stat} \pm 20''_{sys}$. No significantly extended emission could be detected and HESS J1741−302 is found to be a point source with an extension upper limit of 0.068° at a 99% confidence level.

[5] The hotspot structure corresponds to the HESS J1741−302 A region mentioned in e.g. Hare et al. (2016) and Hui et al. (2016).

2.3. Spectral analysis

A circular region with a radius of 0.1° centered at the best fit position of HESS J1741−302 (shown in Fig. 1) was used as an integration region for extracting the VHE γ-ray spectrum of the source, and the reflected background model (Berge et al. 2007) was used for the background estimation. The differential VHE γ-ray spectrum was derived using the forward folding technique (Piron et al. 2001), and is well described (p-value of 0.71) by a simple power-law function $\mathrm{d}N/\mathrm{d}E = \Phi_0\ (E/1\ \mathrm{TeV})^{-\Gamma}$ as shown in Fig. 2. The photon index of HESS J1741−302 is $\Gamma = 2.3 \pm 0.2_{stat} \pm 0.2_{sys}$, while the normalization at 1 TeV is $\Phi_0 = (2.1 \pm 0.4_{stat} \pm 0.4_{sys}) \times 10^{-13}$ cm^{-2} s^{-1} TeV^{-1}. The integral flux level above 1 TeV is $\Phi(>1\ \mathrm{TeV}) = (1.7 \pm 0.3_{stat} \pm 0.3_{sys}) \times 10^{-13}$ cm^{-2} s^{-1} and corresponding to ∼1% of the Crab Nebula flux. The integrated energy flux $F_\gamma(>0.4\ \mathrm{TeV})$ is $\sim 1.2 \times 10^{-12}$ erg cm^{-2} s^{-1}. A power-law function with an exponential cut-off does not statistically improve the fit (0.4σ from LLRT with respect to the power-law function). However, one can not exclude a cut-off in the γ-ray spectrum because of the limited statistics above 10 TeV.

Since this source does not show any significant extension, a variability analysis was performed to test its potential as a binary. The integral flux is found to be constant (p-value of 0.74 for the monthly light curve) within the H.E.S.S. dataset. Variability could be seen neither from run-wise (∼30 min, p-value of 0.99) nor from year-wise (p-value of 0.33) light curves.

3. Study of the interstellar medium

Dense gas regions can provide rich target material for accelerated particles to produce VHE γ-ray emission (Aharonian 1991). For investigating a possible hadronic origin of the emission detected from the direction of HESS J1741−302, the analysis of data from available surveys of atomic and molecular hydrogen around the location of the source has been carried out.

The atomic hydrogen (HI) 21-cm (1420 MHz) spectral line data from the Southern Galactic Plane Survey (SGPS; McClure-Griffiths et al. 2012) and ^{12}CO $J = 1 \rightarrow 0$ rotational transition line emission data from the Nanten Galactic Plane Survey (Mizuno & Fukui 2004) were investigated to determine

Table 3. Properties of interstellar cloud features along the line of sight to HESS J1741−302.

Cloud number	$V_{\rm Int}$ (km/s)	V_p (km/s)	D (kpc)	$M_{\rm cl}$ ($M_\odot$)	$n_{\rm Gas}$ (cm^{-3})	$M_5/D^2_{\rm kpc}$	$k_{\rm CR}$	W_{pp} (erg)
3 (N)	[−31, −18]	−24.2	6.7	6.3×10^4	380	0.0140	53	1.5×10^{47}
1 (N)	[−2, +7]	+2.6	5.0	3.1×10^4	460	0.0125	60	7.0×10^{46}
(CMZ)			8.8	9.7×10^4	260	0.0125	60	3.9×10^{47}
8 (N)	[−221, −210]	−215.7	8.5	6.8×10^4	200	0.0094	79	4.7×10^{47}
2 (N)	[−19, −10]	−15.7	6.0	2.8×10^4	240	0.0078	95	1.9×10^{47}
(F)			11.2	9.8×10^4	130	0.0078	95	1.3×10^{48}
4 (N)	[−51, −47]	−48.8	7.5	2.4×10^4	100	0.0043	174	7.3×10^{47}
5 (N)	[−68, −60]	−64.2	7.7	2.3×10^4	91	0.0039	192	8.5×10^{47}
6 (N)	[−120, −100]	−109.6	8.3	1.9×10^4	62	0.0028	270	1.4×10^{48}
7 (N)	[−145, −165]	−154.6	8.4	2.0×10^4	62	0.0028	262	1.5×10^{48}

Notes. The cloud number column shows the corresponding clouds from Fig. 3, it also indicates whether the cloud is located at a near (N) or far (F) distance. The column labeled $V_{\rm Int}$ shows the velocity integration intervals used to determine the mass of the cloud, while the columns labeled V_p and D give the velocity at which the maximum CO intensity occurs and the distance of the cloud from the Sun, respectively. The $M_{\rm cl}$ column gives the mass of the cloud in terms of solar mass ($M_\odot$), while the column labeled $n_{\rm Gas}$ gives the gas number density of the cloud. The mass uncertainties are around 50%. The M_5/D^2 column gives the γ-ray visibility parameter of the cloud where $M_5 = M_{\rm cl}/10^5\ M_\odot$ is the diffuse mass of the cloud located at a distance $D_{\rm kpc} = D/1$ kpc. The column labeled $k_{\rm CR}$ gives the calculated CR density factor of a cloud, while the W_{pp} column gives the total energy required in protons. The table is sorted according to the descending values of $M_5/D^2_{\rm kpc}$.

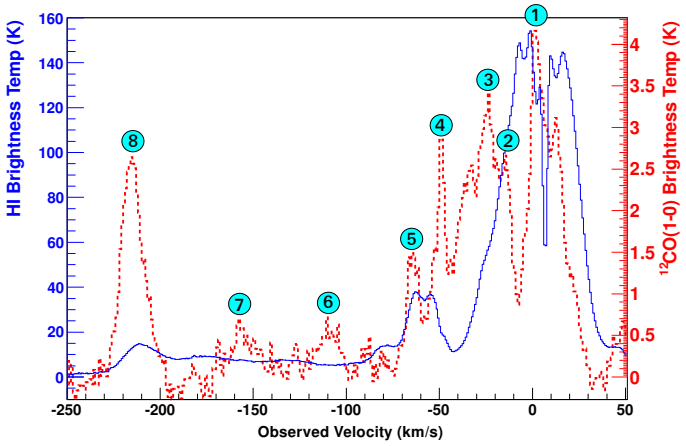

Fig. 3. Brightness temperature distribution of molecular and atomic gas along the line-of-sight to HESS J1741−302. The red dashed line indicates ^{12}CO data from the Nanten survey, while the blue line shows HI data from the SGPS. The profiles are extracted from the circular region with a radius of 0.1° centered on the HESS J1741−302 best fit position. The abscissa shows the observed velocity of gas in km s^{-1}, while the ordinate shows the brightness temperature (the left axis for HI and the right axis for ^{12}CO) in K. Peaks in the ^{12}CO brightness distribution are tagged with a number which indicates the corresponding interstellar cloud feature.

the distribution of atomic and molecular hydrogen in the region of HESS J1741−302. The comparison of HI and ^{12}CO brightness temperature along the line-of-sight is shown in Fig. 3. The velocities of emission maxima (given in Table 3) were used to determine the distances to interstellar cloud features under the assumption of a Galactic rotation curve model (Clemens et al. 1988). These interstellar cloud features will be called "clouds" throughout the text. The near/far kinematic distance ambiguity (KDA) was resolved by using the HI self absorption and 21 cm continuum absorption as explained in e.g. Roman-Duval et al. (2009). Note that the non-zero kinematic velocity of Cloud 1 suggests that it is not far from the Central Molecular Zone (CMZ).

The column densities along the line-of-sight, averaged over the solid angle of the source region, were calculated by integrating the brightness temperature over the velocity intervals covering the observed peaks. The X-factors[6], $X_{\rm HI} = 1.823 \times 10^{18}$ cm^{-2} (K km s^{-1})$^{-1}$ and $X_{^{12}{\rm CO}} = 1.5 \times 10^{20}$ cm^{-2} (K km s^{-1})$^{-1}$, were taken from Dickey & Lockman (1990) and Strong et al. (2004), respectively. Note that the HI X-factor assumes optically thin HI and may underestimate the HI column density by a factor 2−3 (Fukui et al. 2015). The integrated ^{12}CO column density maps are shown in Fig. 4 for each cloud. It was found out that the atomic-to-molecular gas ratio is ∼10%, therefore the molecular gas component dominates. The estimated masses, distances and gas densities for each cloud along the line of sight to HESS J1741−302 are given in Table 3 along with the calculated M_5/D^2 values for the cloud mass to distance squared, one of the principal parameters that determine the γ-ray visibility of a cloud, CR density factors[7] ($k_{\rm CR}$) and total energy in protons (W_{pp}). Note that estimated mass values take into account only the ^{12}CO data. When taking into account the HI data, the mass values increase by a factor of 10%. As shown in Fig. 4, some of the clouds show a good correlation with the VHE emission observed from the direction of HESS J1741−302. The results obtained in this analysis will be used for discussing a possible hadronic scenario (see Sect. 4.1).

4. Discussion

HESS J1741−302 is one of the faintest VHE sources detected so far. Its energy spectrum extending up to at least 10 TeV suggests that the parental particle population producing such emission extends up to tens of TeV in the leptonic case or hundreds of TeV in the hadronic case.

[6] The X-factor is described as the ratio of H_2 column density CO^{12} intensity and the values used throughout this paper are average values in Galactic molecular clouds (Shetty et al. 2011).

[7] CR density factor is the ratio of CR density in a cloud to the one observed at the Earth. See Aharonian (1991) for detailed discussions.

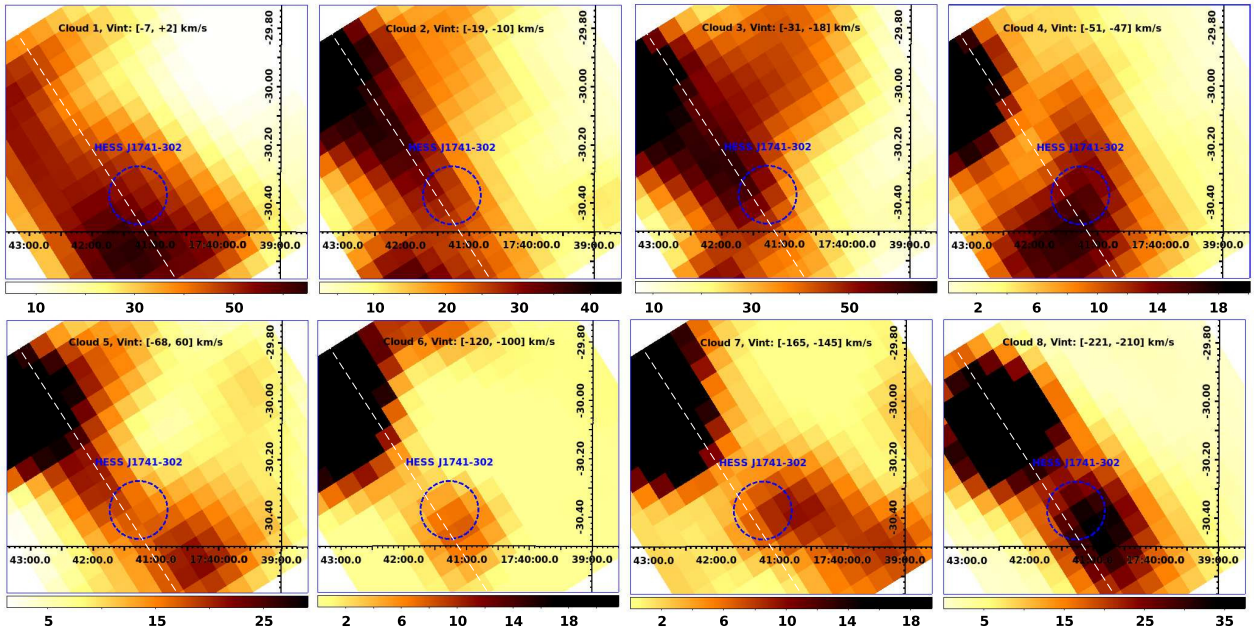

Fig. 4. Integrated ^{12}CO column density maps of the region around HESS J1741−302 for each cloud as labeled in Fig. 3. Velocity integration intervals used for producing the corresponding column density map is given for each cloud. The dashed blue circles show the HESS J1741−302 region which is marked with a dashed black circle in Fig. 1, while the white dashed line indicates the orientation of the Galactic plane. The color scale is in the units of 10^{20} cm^{-2}.

Hereafter, various scenarios to explain the VHE emission from HESS J1741−302 are discussed: a hadronic scenario in which the emission arises from the interaction between an ISM gas target (like a cloud) and accelerated cosmic-rays, and a leptonic scenario, where VHE emission from a relic PWN by electron inverse Compton (IC) scattering off either cosmic microwave background (CMB) photons or infra-red (IR) photons emitted by the OH/IR star. A binary scenario related to the compact radio source 1LC 358.266+00.038, which is coincident with the best fit position of HESS J1741−302, can also be envisaged.

4.1. Hadronic scenarios

The VHE spectrum of HESS J1741−302, extending up to 10 TeV, suggests that the VHE emission could be produced by protons accelerated up to hundreds of TeV colliding with the ambient dense gas. The total energy required in protons, W_{pp}, to produce the inferred γ-ray luminosity, $L_\gamma = 4\pi F_\gamma(>0.4\ \mathrm{TeV})D^2$, can be estimated as $W_{pp} = L_\gamma \times t_{pp}$, where $t_{pp} = 5.76 \times 10^{15} \times (n_{\mathrm{gas}}/\mathrm{cm}^{-3})^{-1}$ s is the cooling time for proton-proton collisions. Calculations of the energy budget suggest that W_{pp} is between 7.0×10^{46} erg and 1.5×10^{48} erg depending on the density of the cloud of interest (see Table 3 for W_{pp} values and cloud distances, D, used for calculating L_γ). Concerning the energy budget, each interstellar cloud found along the line-of-sight to HESS J1741−302 could give rise to the observed VHE emission if an undetected CR source is located in the vicinity of (or inside) one of the clouds. In particular, Cloud 1, Cloud 3 and Cloud 8 in Fig. 4 are promising ISM counterparts for the VHE emission as they partially overlap with HESS J1741−302. However, no established CR accelerator (such as a SNR) is close to, or coincident with, the source.

The results presented in the study of diffuse γ-ray emission from the GC ridge (Aharonian et al. 2006a; H.E.S.S. Collaboration et al. 2016) might suggest that the CRs accelerated by the galactic central source, with an age assumption of ∼10 kyr, can fill the region $|l| < 1°$ but have not yet diffused beyond $|l| \geq 1°$. The projected distance of the Cloud 8 (the closest one to the GC) is 260 pc ± 40 pc (corresponding to $l = -1.7°$). The scenario considering the illumination of Cloud 8 by CRs accelerated at the GC is excluded because of this large offset and since the required CR density factor in this cloud (∼80) is significantly larger than that in the CMZ.

4.2. Leptonic scenarios

Electrons with energies of hundreds of TeV, undergoing IC scattering off CMB or ambient radiation fields, could potentially explain the emission from HESS J1741−302. These electrons could be accelerated at the wind termination shocks of the pulsars around HESS J1741−302 listed in Table 1. Note that pulsars with $\tau_c < 150$ kyr and with $\dot{E}/D^2_{\mathrm{PSR}} \geq 10^{34}$ erg s^{-1} kpc^{-2} are known to power PWNe that are detectable at VHEs (H.E.S.S. Collaboration 2018c). Below, relic PWN scenarios related to the pulsar PSR B1737−30 will be discussed. Note that this pulsar have two distance approximations of 0.4 kpc and 3.28 kpc coming from the absorption of pulsar emission by Galactic HI gas (Verbiest et al. 2012) and the dispersion measure (Taylor & Cordes 1993), respectively. Leptonic VHE emission scenarios related to the other pulsar, PSR J1739−3023, is excluded due to the very large offset of 0.35° with respect to the best fit position of HESS J1741−302.

The angular offset of ∼0.19° between the best fit position of HESS J1741−302 and PSR B1737−30 can be explained with minimum initial pulsar kick velocities of 65 km s^{-1} and 540 km s^{-1} for the pulsar distances of 0.4 kpc and 3.28 kpc, respectively. However, no proper motion in right ascension or in declination is known for this pulsar (Manchester et al. 2005).

A calculation of the characteristic IC cooling time scales suggests that ∼60 TeV electrons can still exist after a time period that corresponds to the characteristic age of the pulsar, while diffusion times of electrons are negligible when compared to this time scale. In such a leptonic scenario, the total energy required

in electrons that gives rise to the inferred γ-ray luminosity can be estimated as W_e ($D_{\rm PSR}$ = 0.4 kpc) = 5.4×10^{44} erg or ∼1%, and $W_e(D_{\rm PSR}$ = 3.28 kpc) = 3.6×10^{46} erg or ∼70% of the maximum energy available from the pulsar when taking into account its age.

In the case of a relic PWN scenario, one expects a (still) bright offset PWN, while the X-ray PWN close to the pulsar is already dim. Although X-ray observations could not detect any X-ray PWN around PSR B1737−30, the phenomenological approach given by Mattana et al. (2009) predicts a faint X-ray PWN around the pulsar with an X-ray flux level[8] of $F(2-10$ keV) = 5.1×10^{-14} erg s^{-1}cm^{-2} for $D_{\rm PSR}$ = 0.4 kpc. Therefore, further targeted X-ray observations of PSR B1737−30 could potentially test the electron accelerator hypothesis.

The spatially coincident compact radio source 1LC 358.266+0.038 is a promising object that can give hints about the nature of HESS J1741−302. Although the spectral index of this source (α = 1.1) is slightly steeper with respect to the indices ($0.2 \leq \alpha \leq 1.0$) suggested by Fender (2001), a γ-ray binary origin could be envisaged as it was done for the γ-ray binary LS 5039 (Marcote et al. 2015), while Pynzar & Shishov (2014) classified this object as extragalactic. In view of the point-like nature of HESS J1741−302 and given the low statistics, the fact that no variability has been observed can not be taken as evidence for disfavoring a binary origin, while scenarios related to the extragalactic origin of the source are highly unlikely when taking into account that the observed VHE emission is located in the Galactic plane, ∼1.7° away from the Galactic center.

Other leptonic scenarios can be considered taking into account the stars in the vicinity of HESS J1741−302. In such scenarios, the strong IR photon field of OH 358.23+0.11 can provide target photons for the production of IC scattered γ-rays in the presence of relativistic electron populations provided by PSR B1737−30 in a putative OH/IR star – pulsar system. Alternatively, VHE γ-ray emission scenarios related to the ∼1.5 yr period binary star WR 98a can be discussed. In both of these cases, one expects that the center-of-gravity of the VHE γ-ray excess must be coincident with the region where VHE electron acceleration takes place. Using this argument, VHE γ-ray emission scenarios related to WR 98a and OH 358.23+0.11 are disfavored in the light of significant offsets (∼0.16° and ∼0.08° respectively) between these stars and the best fit position of HESS J1741−302. The LBV star Wray 17−96, located at a distance of 4.5 kpc, has an offset of ∼0.27° from the best fit position of HESS J1741−302 and can be excluded from the scenarios related to the origin of the source. On the other hand, this extremely rare type of star is located ∼1.1σ away from the best fit position of the hotspot structure.

5. Conclusions

H.E.S.S. has discovered a new unidentified VHE γ-ray source HESS J1741−302 in the Galactic plane. The analysis of H.E.S.S. data has shown that the γ-ray spectrum of HESS J1741−302 extends at least up to 10 TeV. Hadronic particles accelerated up to hundreds of TeV by an undetected cosmic-ray source interacting with the detected clouds along the line-of-sight to HESS J1741−302 can result in the observed VHE γ-ray emission, in particular, Cloud 1, Cloud 3 and Cloud 8 are promising candidates (see Sect. 3). On the other hand, a relic PWN scenario related to the pulsar PSR B1737−30 located at 0.4 kpc can not be excluded but is disfavoured due to the point-like nature of the source and its offset with respect to the pulsar. Future X-ray observations of this pulsar can be used for testing such a relic PWN scenario. A binary scenario related to the compact radio source 1LC 358.266+0.038 is also possible. Despite a thorough investigation of its multi-wavelength environment and consideration of a variety of plausible emission mechanisms, this enigmatic VHE source remains unidentified. The future Cherenkov Telescope Array with its much better angular resolution and sensitivity will be able to further characterize the VHE γ-ray emission from this region.

Acknowledgements. The support of the Namibian authorities and of the University of Namibia in facilitating the construction and operation of H.E.S.S. is gratefully acknowledged, as is the support by the German Ministry for Education and Research (BMBF), the Max Planck Society, the German Research Foundation (DFG), the Alexander von Humboldt Foundation, the Deutsche Forschungsgemeinschaft, the French Ministry for Research, the CNRS-IN2P3 and the Astroparticle Interdisciplinary Programme of the CNRS, the UK Science and Technology Facilities Council (STFC), the IPNP of the Charles University, the Czech Science Foundation, the Polish National Science Centre, the South African Department of Science and Technology and National Research Foundation, the University of Namibia, the National Commission on Research, Science & Technology of Namibia (NCRST), the Innsbruck University, the Austrian Science Fund (FWF), and the Austrian Federal Ministry for Science, Research and Economy, the University of Adelaide and the Australian Research Council, the Japan Society for the Promotion of Science and by the University of Amsterdam. We appreciate the excellent work of the technical support staff in Berlin, Durham, Hamburg, Heidelberg, Palaiseau, Paris, Saclay, and in Namibia in the construction and operation of the equipment. This work benefited from services provided by the H.E.S.S. Virtual Organisation, supported by the national resource providers of the EGI Federation. This research has made use of software provided by the *Chandra* X-ray Center (CXC) in the application packages CIAO, ChIPS, and Sherpa. This research has made use of the SIMBAD database, operated at CDS, Strasbourg, France. This research has made use of the ATNF pulsar catalog database (http://www.atnf.csiro.au/research/pulsar/psrcat/). The NANTEN project is based on the mutual agreement between Nagoya University and the Carnegie Institution of Washington. Sabrina Casanova and Ekrem Oğuzhan Angüner acknowledge the support from the Polish National Science Center under the Opus Grant UMO-2014/13/B/ST9/00945.

References

Acero, F., Ackermann, M., Ajello, M., et al. 2015, ApJS, 218, 23
Ackermann, M., Ajello, M., Atwood, W. B., et al. 2016, ApJS, 222, 5
Aharonian, F. 1991, Ap&SS, 180, 305
Aharonian, F., Akhperjanian, A. G., Bazer-Bachi, A. R., et al. 2006a, Nature, 439, 695
Aharonian, F., Akhperjanian, A. G., Bazer-Bachi, A. R., et al. 2006b, ApJ, 636, 777
Aharonian, F., Akhperjanian, A. G., Bazer-Bachi, A. R., et al. 2006c, A&A, 457, 899
Berge, D., Funk, S., & Hinton, J. 2007, A&A, 466, 1219
Bolmont, J., Corona, P., Gauron, P., et al. 2014, Nucl. Instr. Meth. Phys. Res. A, 761, 46
Burrows, D. N., Hill, J. E., Nousek, J. A., et al. 2005, Space Sci. Rev., 120, 165
Caswell, J. L. 1998, MNRAS, 297, 215
Clark, J. S., Larionov, V. M., & Arkharov, A. 2005, A&A, 435, 239
Clemens, D. P., Sanders, D. B., & Scoville, N. Z. 1988, ApJ, 327, 139
Cutri, R. M., Skrutskie, M. F., van Dyk, S., et al. 2003, VizieR Online Data Catalog, II/246
De Becker, M., & Raucq, F. 2013, A&A, 558, A28
Dickey, J. M., & Lockman, F. J. 1990, ARA&A, 28, 215
Fender, R. P. 2001, MNRAS, 322, 31
Freeman, P., Doe, S., & Siemiginowska, A. 2001, Proc. SPIE, 4477, 76
Fukui, Y., Torii, K., Onishi, T., et al. 2015, ApJ, 798, 6
Hare, J., Rangelov, B., Sonbas, E., Kargaltsev, O., & Volkov, I. 2016, ApJ, 816, 52
H.E.S.S. Collaboration (Abdalla, H., Abramowski, A., et al.) 2016, Nature, 531, 476

[8] This flux level is estimated by using $\dot{E}$ and it increases to $F(2-10$ keV) = 1.4×10^{-13} erg s^{-1} cm^{-2} when τ_c is taken into account. These expectations are compatible with flux upper limits given in Uchiyama et al. (2011).

H.E.S.S. Collaboration (Abdalla, H., Abramowski, A., et al.) 2018a, A&A, 612, A11 (H.E.S.S. SI)
H.E.S.S. Collaboration (Abdalla, H., Abramowski, A., et al.) 2018b, A&A, 612, A1 (H.E.S.S. SI)
H.E.S.S. Collaboration (Abdalla, H., Abramowski, A., et al.) 2018c, A&A, 612, A2 (H.E.S.S. SI)
Hui, C. Y., Yeung, P. K. H., Ng, C. W., et al. 2016, MNRAS, 457, 4262
Li, T.-P., & Ma, Y.-Q. 1983, ApJ, 272, 317
Manchester, R. N., Hobbs, G. B., Teoh, A., & Hobbs, M. 2005, ApJ, 129, 1993
Marcote, B., Ribó, M., Paredes, J. M., & Ishwara-Chandra, C. H. 2015, MNRAS, 451, 59
Mattana, F., Falanga, M., Götz, D., et al. 2009, ApJ, 694, 12
McClure-Griffiths, N. M., Dickey, J. M., Gaensler, B. M., et al. 2012, ApJS, 199, 12
Mitsuda, K., Bautz, M., Inoue, H., et al. 2007, PASJ, 59, S1
Mizuno, A., & Fukui, Y. 2004, in Proc. ASP. Conf., 317, 59
Monnier, J. D., Tuthill, P. G., & Danchi, W. C. 1999, ApJ, 525, L97
Nord, M. E., Lazio, T. J. W., Kassim, N. E., et al. 2004, AJ, 128, 1646
Ohm, S., van Eldik, C., & Egberts, K. 2009, Astropart. Phys., 31, 383
Piron, F., Djannati-Ataï, A., Punch, M., et al. 2001, A&A, 374, 895
Pynzar, A. V., & Shishov, V. I. 2014, Astron. Rep, 58, 427
Roman-Duval, J., Jackson, J. M., Heyer, M., et al. 2009, ApJ, 699, 1153
Schwartz, D. A. 2004, Int. J. Mod. Phys. D, 13, 1239
Shetty, R., Glover, S. C., Dullemond, C. P., et al. 2011, MNRAS, 415, 3253
Strong, A. W., kalenko, I. V. M., Reimer, O., Digel, S., & Diehl, R. 2004, A&A, 422, L47
Taylor, J. H., & Cordes, J. M. 1993, ApJ, 411, 674
Tibolla, O., Komin, N., Kosack, K., & Naumann-Godo, M. 2008, AIP Conf. Proc., 1085, 249
Uchiyama, H., Koyama, K., Matsumoto, H., et al. 2011, PASJ, 63, S865
Verbiest, J. P. W., Weisberg, J. M., Chael, A. A., Lee, K. J., & Lorimer, D. R. 2012, ApJ, 755, 39

[1] Centre for Space Research, North-West University, 2520 Potchefstroom, South Africa
[2] Universität Hamburg, Institut für Experimentalphysik, Luruper Chaussee 149, 22761 Hamburg, Germany
[3] Max-Planck-Institut für Kernphysik, PO Box 103980, 69029 Heidelberg, Germany
[4] Dublin Institute for Advanced Studies, 31 Fitzwilliam Place, Dublin 2, Ireland
[5] National Academy of Sciences of the Republic of Armenia, Marshall Baghramian Avenue, 24, 0019 Yerevan, Republic of Armenia
[6] Yerevan Physics Institute, 2 Alikhanian Brothers St., 375036 Yerevan, Armenia
[7] Institut für Physik, Humboldt-Universität zu Berlin, Newtonstr. 15, 12489 Berlin, Germany
[8] University of Namibia, Department of Physics, Private Bag, 13301 Windhoek, Namibia
[9] GRAPPA, Anton Pannekoek Institute for Astronomy, University of Amsterdam, Science Park 904, 1098 XH Amsterdam, The Netherlands
[10] Department of Physics and Electrical Engineering, Linnaeus University, 351 95 Växjö, Sweden
[11] Institut für Theoretische Physik, Lehrstuhl IV: Weltraum und Astrophysik, Ruhr-Universität Bochum, 44780 Bochum, Germany
[12] GRAPPA, Anton Pannekoek Institute for Astronomy and Institute of High-Energy Physics, University of Amsterdam, Science Park 904, 1098 XH Amsterdam, The Netherlands
[13] Institut für Astro- und Teilchenphysik, Leopold-Franzens-Universität Innsbruck, 6020 Innsbruck, Austria
[14] School of Physical Sciences, University of Adelaide, 5005 Adelaide, Australia
[15] LUTH, Observatoire de Paris, PSL Research University, CNRS, Université Paris Diderot, 5 Place Jules Janssen, 92190 Meudon, France
[16] Sorbonne Universités, UPMC Université Paris 06, Université Paris Diderot, Sorbonne Paris Cité, CNRS, Laboratoire de Physique Nucléaire et de Hautes Energies (LPNHE), 4 place Jussieu, 75252 Paris Cedex 5, France
[17] Laboratoire Univers et Particules de Montpellier, Université Montpellier, CNRS/IN2P3, CC 72, Place Eugène Bataillon, 34095 Montpellier Cedex 5, France
[18] IRFU, CEA, Université Paris-Saclay, 91191 Gif-sur-Yvette, France
[19] Astronomical Observatory, The University of Warsaw, Al. Ujazdowskie 4, 00-478 Warsaw, Poland
[20] Aix Marseille Université, CNRS/IN2P3, CPPM, Marseille, France
[21] Instytut Fizyki Jądrowej PAN, ul. Radzikowskiego 152, 31-342 Kraków, Poland
[22] Funded by EU FP7 Marie Curie, grant agreement No. PIEF-GA-2012-332350
[23] School of Physics, University of the Witwatersrand, 1 Jan Smuts Avenue, Braamfontein, 2050 Johannesburg, South Africa
[24] Laboratoire d'Annecy de Physique des Particules, Université Savoie Mont-Blanc, CNRS/IN2P3, 74941 Annecy-le-Vieux, France
[25] Landessternwarte, Universität Heidelberg, Königstuhl, 69117 Heidelberg, Germany
[26] Université Bordeaux, CNRS/IN2P3, Centre d'Études Nucléaires de Bordeaux Gradignan, 33175 Gradignan, France
[27] Oskar Klein Centre, Department of Physics, Stockholm University, Albanova University Center, 10691 Stockholm, Sweden
[28] Institut für Astronomie und Astrophysik, Universität Tübingen, Sand 1, 72076 Tübingen, Germany
[29] Laboratoire Leprince-Ringuet, Ecole Polytechnique, CNRS/IN2P3, 91128 Palaiseau, France
[30] APC, AstroParticule et Cosmologie, Université Paris Diderot, CNRS/IN2P3, CEA/Irfu, Observatoire de Paris, Sorbonne Paris Cité, 10, rue Alice Domon et Léonie Duquet, 75205 Paris Cedex 13, France
[31] Univ. Grenoble Alpes, CNRS, IPAG, 38000 Grenoble, France
[32] Department of Physics and Astronomy, The University of Leicester, University Road, Leicester, LE1 7RH, UK
[33] Nicolaus Copernicus Astronomical Center, Polish Academy of Sciences, ul. Bartycka 18, 00-716 Warsaw, Poland
[34] Institut für Physik und Astronomie, Universität Potsdam, Karl-Liebknecht-Strasse 24/25, 14476 Potsdam, Germany
[35] Friedrich-Alexander-Universität Erlangen-Nürnberg, Erlangen Centre for Astroparticle Physics, Erwin-Rommel-Str. 1, 91058 Erlangen, Germany
[36] DESY, 15738 Zeuthen, Germany
[37] Obserwatorium Astronomiczne, Uniwersytet Jagielloński, ul. Orla 171, 30-244 Kraków, Poland
[38] Centre for Astronomy, Faculty of Physics, Astronomy and Informatics, Nicolaus Copernicus University, Grudziadzka 5, 87-100 Torun, Poland
[39] Department of Physics, University of the Free State, PO Box 339, 9300 Bloemfontein, South Africa
[40] Heisenberg Fellow (DFG), ITA Universität Heidelberg, Germany
[41] Department of Physics, Rikkyo University, 3-34-1 Nishi-Ikebukuro, Toshima-ku, 171-8501 Tokyo, Japan
[42] Japan Aerospace Exploration Agency (JAXA), Institute of Space and Astronautical Science (ISAS), 3-1-1 Yoshinodai, Chuo-ku, Sagamihara, Kanagawa 229-8510, Japan
[43] Now at The School of Physics, The University of New South Wales, 2052 Sydney, Australia
[44] Now at Instituto de Física de São Carlos, Universidade de São Paulo, Av. Trabalhador São-carlense, 400 – CEP 13566-590, São Carlos, SP, Brazil
[45] Now at Kavli Institute for Particle Astrophysics and Cosmology, Department of Physics and SLAC National Accelerator Laboratory, Stanford University, Stanford, 94305 California, USA
[46] Department of Physics, Nagoya University, Furo-cho, Chikusa-ku, 464-8601 Nagoya, Japan
[47] Nobeyama Radio Observatory, Minamimaki, Minamisaku, 384-1805 Nagano, Japan